TRENDS IN SCIENCES 2026; 23(3): 11568
https://doi.org/10.48048/tis.2026.11568 RESEARCH ARTICLE

Ultrasound-Assisted Encapsulation of Curcumin: RSM Optimization and Release Kinetics

Aji Prasetyaningrum*, Aulia Dwi Ashianti, Nur Rokhati, Moh Djaeni, Ratnawati Ratnawati and Dani Puji Utomo

Department of Chemical Engineering, Faculty of Engineering, Diponegoro University, Semarang 50275, Indonesia

(***Corresponding author's e-mail: aji.prasetyaningrum@che.undip.ac.id)**

Received: 11 August 2025, Revised: 20 September 2025, Accepted: 3 October 2025, Published: 10 December 2025

Abstract

Curcumin is a bioactive compound with strong antioxidant properties, yet its application is limited by low aqueous solubility and instability against chemical and metabolic degradation. To enhance its functional performance, curcumin was encapsulated using alginate-chitosan as wall materials assisted by ultrasonic homogenization. Process optimization was conducted through Response Surface Methodology (RSM) with Central Composite Design (CCD), considering sonication time (X_1) and ultrasonic power (X_2) as independent variables. The analysis of the optimization process demonstrated that the maximum encapsulation efficiency and swelling ratio were realized after 10 min of sonication at a power of 210 W. Compared to the non-ultrasonicated microcapsule, ultrasound treatment significantly enhanced encapsulation efficiency, reduced particle size, and improved homogeneity of the emulsion. Characterization using FTIR confirmed stronger molecular interactions between alginate, chitosan, and curcumin under ultrasound conditions, while SEM micrographs showed rougher surfaces with cracks that facilitated structural integrity. Particle size analysis (PSA) indicated a narrower and more uniform size distribution in the ultrasound-treated samples. Furthermore, the release kinetics analysis was well-fitted to the Peppas-Sahlin model, suggesting a dominant diffusion-controlled mechanism. These results indicate that ultrasonic treatment plays a role in influencing the encapsulation properties of curcumin, although further research is needed to fully understand its effect on the release profile of bioactive substances.

Keywords: Encapsulation, Curcumin, Alginate, Optimization, Ultrasound

Introduction

Curcumin, also known as diferuloylmethane (1,7-bis(4-hydroxy-3-methoxyphenyl)-1,6-heptadiene-3,5-dione), is a hydrophobic polyphenol obtained from the rhizomes of *Curcuma spp.* and has different bioactive properties. Alongside their structural analogue, collectively referred to as curcuminoids, they display robust antioxidant, anti-inflammatory, antimicrobial, and anticarcinogenic attributes with low oral toxicity [1]. The poor water solubility and sensitivity of curcumin to chemical and metabolic degradation, which results in restricted oral bioavailability, makes it difficult to formulate it as a medicinal drug. Several strategies such as encapsulation have been proposed to overcome these limitations [2].

Encapsulation is a widely used technique that involves covering a substance with an external membrane or coating to prevent biochemical and thermal deterioration of volatile, bioactive, and rapidly degradable substances [3]. This technique enhances the physical activity, solubility, and bioavailability of bioactive compounds [4]. During encapsulation, the enclosed substance is known as the core material, whereas the substance encapsulating it is referred to as the carrier or coating material. The core material may comprise a mixture of active constituents, stabilizers, diluents, or accelerators. Coating materials, derived from natural or synthetic polymers, form cohesive films with properties such as strength, flexibility, impermeability, optical characteristics, and stability against the core material [5].

Alginate is commonly used in various biomedical applications including drug delivery, tissue engineering, and formulation to prevent gastric reflux [6]. Alginate can form hydrogels using a variety of cross-linking techniques, such as ionic modification, which is based on the ability of guluronate to bind cations ("egg-box" model) [7]. Pure alginate hydrogels exhibit a low viscoelasticity and high permeability. Composite hydrogels of alginate with other natural and synthetic polymers have been utilized to enhance its physicochemical properties. Alginate effortlessly forms a polyelectrolyte complex with polycations, such as chitosan, demonstrating synergistic chemical, rheological, and mechanical properties. These hydrogels show promise for encapsulating drugs, oligonucleotides, proteins, and cells. Over a wide pH range, these polymer combinations yielded strong composite hydrogels with notable mechanical strength and viscoelastic characteristics [8]. Moreover, the alginate-chitosan complex yielded smaller particles, increasing the specific surface area for enhanced drug absorption on the epithelial surface [9].

The process of encapsulating bioactive compounds depends on the formation of a complex coacervation between polysaccharides and proteins. This interaction involves intermolecular interactions, such as hydrogen bonding, electrostatic repulsion, and surface hydrophilicity [10]. Multiple encapsulation methods exist for enclosing the active ingredients, and each method influences the final characteristics and microparticle properties [11]. Among these methods, spray drying is a commonly used technique for food encapsulation, which requires wall materials with excellent water solubility and heat resistance; however, its use may lead to agglomeration issues [12]. In contrast, freeze-drying, although simpler than other techniques, entails high costs and remains prevalent for producing high-value food products [13,14]. Despite challenges in scalability and reduced post-process viability, extrusion is based on passing a polymer solution with active ingredients through a nozzle into a gelling solution [14,15]. Coacervation, especially the complex coacervation method, offers stability under various conditions, such as high coating activity, humidity, elevated temperatures, and controlled release in the gastrointestinal system; however, its limited use in the food industry is due to complexity and cost factors [12].

Ionic gelation has been used to synthesize polymer micro-and nanoparticles for biomedical applications. This method is relatively simple and flexible for the production of particles of various sizes [16]. Among the advantages and disadvantages of encapsulation methods, the ionic gelation method is intriguing for further development, as it effectively protects bioactive compounds, is non-toxic, and is environmentally friendly. Encapsulation using ionic gelation method typically begins with the formation of an emulsion of bioactive substances with a wall material. The formation of core-shell materials in ionic gelation techniques is typically elaborate. Furthermore, core-shell materials synthesized using the ionic gelation method have been reported to have low stability and larger and non-homogeneous droplet sizes [17]. Ultrasonic treatment can be used to address the challenges associated with ionic gelation. Ultrasonics have been effective in significantly reducing emulsion droplet sizes to the nanoscale level [18].

Ultrasounds, produced by piezoelectric transducers that convert electrical pulses into acoustic energy waves, induce cavitation and form gas bubbles. This cavitation effect breaks oil droplets into smaller sizes [19]. Ultrasound considerably reduces homogenization time compared to conventional methods, leading to improved flavour encapsulation in the wall material [20]. Numerous studies have confirmed the significant effects of ultrasound on protein particle size, uniformity [21], charge [22], conformational changes, sensitivity to enzymatic hydrolysis [21], and functional properties [23]. Additionally, ultrasound alters the structure and functional properties of polysaccharides, enhancing various characteristics, such as antioxidant, anticoagulant, prebiotic, anti-inflammatory, and physicochemical traits [24].

This study introduces a novel method to improve the quality of curcumin microencapsulation using ultrasonic-assisted homogenization conditions. Furthermore, the optimization of ultrasonication technology for curcumin encapsulation has not been widely performed. This study employed Response Surface Methodology (RSM) using a Central Composite Design (CCD) to systematically optimize sonication

parameters, specifically time and power, to simultaneously improve the encapsulation efficiency and swelling ratio of the resulting microcapsules. The use of ultrasonication not only reduced the droplet size and improved the emulsion uniformity but also overcame the inherent limitations of ionic gelation, such as poor stability and large and heterogeneous particle size. Furthermore, this study presents a comprehensive characterization of microcapsules through SEM, FTIR, and particle size analysis, and evaluates the release profile of encapsulated curcumin. These results provide a basis for the development of controlled-release delivery systems for food and pharmaceutical applications.

Materials and methods

Materials

Curcumin extract was obtained from SIGMA-Aldrich, alginate (molar mass 216.12 g/mol with CAS Number 9005-38-3 SIGMA-Aldrich, USA), chitosan (75% - 85% degree of deacetylation, molar mass 50,000 - 190,000 Da with CAS Number 9012-76-4 SIGMA Aldrich, USA), soybean oil was obtained from Sania Royale Oil (PT Wilmar Internasional, Indonesia), acetic acid (CAS Number 64-19-7 SIGMA Aldrich, USA), tween 80 (CAS Number 9005-65-6 SIGMA Aldrich, USA), and calcium chloride (CAS Number 10043-52-4 SIGMA Aldrich, USA).

Preparation of the curcumin microcapsule

The encapsulation process involves a 2-step procedure for particle preparation. Initially, sodium alginate (2 %w/v) was dissolved in 100 mL of distilled water and stirred at 500 rpm for 45 min at approximately ± 30 °C. Simultaneously, a curcumin solution was prepared by mixing 1% weight of curcumin extract with 30 mL of soybean oil until a homogeneous mixture was obtained. Subsequently, 0.5% Tween 80 and curcumin oil were added to the alginate solution. The combined solution were continuously mixed using a homogenizer for 20 min. Subsequently, the solution underwent sonication using ultrasound (Biostellar BSD 650 W) at various time intervals (6 - 12 min) and power levels (100 - 300 W). In the second step, chitosan (1 %w/v) was dissolved in 100 mL acetic acid solution at pH 5 and stirred at 500 rpm for 45 min at approximately ± 30 °C. The chitosan solution was then added to the solution obtained in the first step at a volume ratio of 1:1 (v/v). The resulting mixture was homogenized for 15 min until a uniform solution was obtained. This homogenous solution was then injected into a 0.2 M $CaCl_2$ solution while being constantly stirred. The formed particles were allowed to remain in the cross-linking solution for 30 min to ensure stabilization. Subsequently, they were separated via filtration and dried at room temperature for 48 h.

Encapsulation efficiency

Encapsulation efficiency was assessed by quantifying the quantity of bioactive substances that remained unconfined within the alginate-chitosan beads after immersion in a $CaCl_2$ solution. In this instance, the encapsulation efficiency is denoted as:

$$EE\ (\%) = \frac{Qt - Qr}{Qt} \times 100 \quad (1)$$

where Qt is the quantity of bioactive curcumin and Qr is the bioactive curcumin present in the $CaCl_2$ solution after encapsulation. Calculations were conducted in triplicate.

Swelling analysis

The swelling was assessed using a pH 7 buffer solution. The swelling percentage was calculated using the following formula:

$$\text{Swelling ratio} = \frac{W_s - W_d}{W_d} \quad (2)$$

where W_s represents the weight of the bead when wet and W_d denotes the weight of the bead when dry. Calculations were conducted in triplicates.

Particle size analysis

The particle size was measured using a Laser Particle Size Analyzer (PSA) LLPA-C10. Initially, samples were weighed and placed in a cuvette. The Aqua Pro injection was added to a cuvette containing the sample. Subsequently, a cuvette containing the sample and aqua pro injection was inserted into the tool holder of the Particle Size Analyzer for analysis.

SEM analysis

The surface structure of the curcumin-encapsulated material was investigated using a SEM JEOL JSM-6510LA instrument. Before conducting the analysis, the samples were subjected to gold metallization using a sputter-coating unit. During the examination, the SEM was set to a magnification of 1.500× to observe the surface morphology of the samples.

FTIR analysis

The best encapsulation outcomes were examined using a Perkin Elmer Spectrum IR 10.6.1 spectrophotometer (Perkin Elmer Inc., US). This analysis aimed to identify the functional groups present and characterize their properties within the spectral range of 4,000 - 400 cm^{-1}.

Curcumin release kinetics study

The release of bioactive curcumin during encapsulation was investigated in pH 1.2 and 6.8 solution. A full 24 h of immersion was required for 0.2 g of the best formulation of encapsulated curcumin in 30 mL of a pH-different solution. To determine the bioactive release in curcumin at each time interval, 5 mL of the sample was analyzed using a spectrophotometer Genesys 50 UV-Vis at a wavelength of 423 nm. Three different mathematical models were used to determine the mechanism of curcumin release from the beads. To calculate all models, experimental data were required from the amount of bioactive compounds released at equilibrium time (M_{eq}) and time t (M_t), which was then calculated using the following the empirical equation:

Higuchi model:

$$\frac{M_t}{M_{eq}} = k_h t^{0.5} \quad (3)$$

where k_h denotes the Higuchi coefficient. If the correlation coefficient value is high for the fitting, it can be interpreted that the main mechanism of the release of bioactive compounds is the diffusion release mechanism [25].

Ritger-Peppas model:

$$\frac{M_t}{M_{eq}} = k_1 t^n \quad (4)$$

where k_1 denotes the release rate constant based on the structural and geometric characteristics of the release system and n is the diffusion exponent. If $n \leq 0.43$, the release mechanism is a molecular-diffusion-based bioactive compound release mechanism, whereas if $n \geq 0.85$, it is a relaxation-based bioactive compound release mechanism during bioactive transport, which includes tension and state transitions in the polymer swells in water. If $0.43 < n < 0.85$, the release of bioactive compounds is controlled by diffusion, followed by relaxation [25].

Peppas-Sahlin model:

$$\frac{M_t}{M_{eq}} = k_1 t^m + k_2 t^{2m} \quad (5)$$

This release kinetics model was applied to the diffusion and relaxation release mechanisms in curcumin release processes. The F value represents the contribution of Fickian diffusion to the release of a bioactive compound, whereas the R value represents the relaxation contribution. The R/F ratio indicates the contribution of relaxation and Fickian diffusion to the drug release. When R/F = 1, erosion (relaxation) and diffusion contribute equally to the release mechanism. If R/F > 1, relaxation (erosion) dominates, while for R/F < 1, diffusion dominates. The relaxation ratio (R) vs. the Fickian contribution (F) was calculated as follows:

$$\frac{R}{F} = \frac{k_2}{k_1} t^m \quad (6)$$

where k_2 is the relaxation kinetic constant obtained from the Peppas-Sahlin equation and k_1 is the Fickian diffusion rate constant [25].

Experimental design and process optimization

In the initial stage, pre-optimization screening was carried out at sonication time range of 0 - 15 min and power of 0 - 500 W to determine the variable limits. Response Surface Methodology (RSM) using a Central Composite Design (CCD) was employed to investigate the relationship between 2 variables (ultrasound time and power). The experimental design is summarized in **Table 1**. The variations in time (X_1) and power (X_2) of sonication were chosen as independent variables. The

independent variables were set at a sonication time of 6 - 12 min and a sonication power of 100 - 300 W. For a combination of independent factors, the encapsulation efficiency and swelling degree were chosen as the responses. The real values of the independent variables must be translated into coded variables (−1, 0 and +1) for analysis using the response surface approach. Statistica 6.0 software was used to carry out the RSM/CCD study.

Table 1 Independent variable from design of experiment (DoE).

Run	Variable		Code	
	Time (min)	Power (W)	X_1	X_2
1	6	100	−1	−1
2	6	300	−1	1
3	12	100	1	−1
4	12	300	1	1
5	4.8	200	−1.414	0
6	13.2	200	1.414	0
7	9	59	0	−1.414
8	9	341	0	1.414
9	9	200	0	0
10	9	200	0	0
11	9	200	0	0
12	9	200	0	0
13	9	200	0	0

Results and discussion

Effect of time and power sonication of curcumin encapsulation

The encapsulation of curcumin by ultrasound treatment was conducted to analyze the encapsulation efficiency and swelling to examine the impact of ultrasound time on these factors. The effects of ultrasound time and power on encapsulation efficiency were evaluated over a time range of 0 - 15 min (**Figure 1(a)**). The results showed that optimum encapsulation efficiency and swelling ratio were obtained after 9 min of sonication. Ren *et al.* [26] reported that ultrasonication can significantly improve the encapsulation efficiency with increasing sonication time. Acoustic cavitation generated by ultrasonic waves can alter macromolecular structures and enhance macromolecular interactions. The mechanical effect of acoustic cavitation can also increase the mass transfer rate, contact frequency, and collisions between the shell and core, thereby enhancing encapsulation efficiency [27]. Although increasing the sonication time can enhance encapsulation efficiency, Huang *et al.* [28] suggested that an increase in sonication time may lead to a decrease in encapsulation efficiency. The ultrasonic cavitation effect may increase the probability of droplet rupture and delamination of the core-shell structure of composite particles, resulting in more loaded drug leakage and reduced encapsulation efficiency.

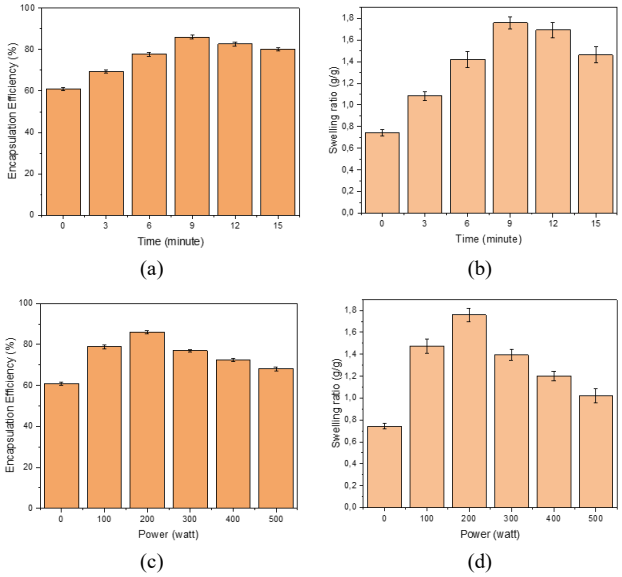

Figure 1 Effect of sonication time and power on encapsulation efficiency and swelling ratio.

Furthermore, **Figure 1(b)** shows the effect of ultrasonication time on the swelling ratio. In the range of 0 - 9 min, the swelling ratio increased from 0.74 g/g to a maximum of 1.76 g/g. However, at 12 - 15 min, the value decreased from 1.69 to 1.46 g/g. With increasing ultrasound duration, the swelling ratio initially increased and then decreased. The increase in duration triggered the thermal effect of ultrasonic waves, promoting intermolecular motion and exposing hydrophilic groups, so that the swelling ratio increased to an optimum point [29]. However, excessive ultrasound processing can result in the merging of previously formed droplets, which is known as recoalescence. This phenomenon diminishes the efficacy of encapsulation and leads to an increase in droplet size, thereby reducing the ability of the particle to swell effectively [30]. The swelling ratio typically increased as the particle size decreased [31].

In **Figure 1(c)**, it can be observed that within the power range of 0 - 200 W. The highest encapsulation efficiency of 85.98% was achieved at 200 W. Ren *et al.* [26] stated that ultrasonication can significantly enhance encapsulation efficiency with increasing sonication power. Acoustic cavitation and the mechanical effects of acoustic cavitation played a role in this improvement. However, an increase in sonication power can also lead to a decrease in encapsulation efficiency owing to the ultrasonic cavitation effect, increasing the probability of droplet rupture and delamination of the core-shell structure of the composite particles [28].

Figure 1(d) illustrates the influence of ultrasonication power on the swelling ratio. Within the power range of 0 - 200 W, the ratio rose from 0.74 to 1.76 g/g. In contrast, at a higher power level of 300 - 500 W, the ratio decreased from 1.55 to 1.02 g/g. Increasing the ultrasonication power tends to enhance the swelling ratio owing to increased sonic cavitation [32]. However, excessive ultrasound processing can result in the merging of previously formed droplets, which is known as recoalescence. This phenomenon diminishes the efficacy of encapsulation and leads to an increase in droplet size, thereby reducing the ability of particles to swell effectively [30]. The swelling ratio typically increased as the particle size decreased [31].

Prediction adequacy of models

Curcumin was encapsulated into alginate-chitosan beads assisted by ultrasound. Subsequently, RSM was used to fine-tune the operating parameters of the time (X_1) and power (X_2). The experimental error (pure error) and data reproducibility were determined using the center point (run 9 - 13). To predict the encapsulation efficiency and swelling ratio, 2 equations, including 1st order (linear) and 2nd order (quadratic), were assessed. **Table 2** shows a comparison of the linear and quadratic results in predicting the encapsulation efficiency and swelling ratio with respect to the sum of squares analysis.

Table 2 Experimental design optimized encapsulation efficiency and swelling ratio using ultrasound.

Run	Time (min)	Power (W)	Experimental values		Predicted values	
			%EE	Swelling ratio (g/g)	%EE	Swelling ratio (g/g)
1	6	100	70.281	1.221	70.477	1.229
2	6	300	71.515	1.249	71.759	1.245
3	12	100	75.613	1.377	75.438	1.382
4	12	300	79.277	1.545	79.151	1.539
5	4.8	200	72.984	1.354	72.687	1.351
6	13.2	200	81.193	1.666	81.421	1.667
7	9	59	69.592	1.137	69.592	1.128
8	9	341	73.194	1.242	73.125	1.250
9	9	200	85.678	1.757	85.947	1.752
10	9	200	85.976	1.754	85.947	1.752
11	9	200	86.356	1.747	85.947	1.752
12	9	200	85.559	1.746	85.947	1.752
13	9	200	86.163	1.755	85.947	1.752

Table 3 Sum of square in the analysis of variance of encapsulation efficiency and swelling ratio.

Dependent variables	Source	Sum of squares	dF	Mean Square	F value	*p*-value	R^2	
%EE	Quadratic	455.1	2	227.55	2436.65	< 0.0001	0.9988	Suggested
	Cubic	0.2804	2	0.1402	1.88	0.2465	0.9993	Aliased
Swelling ratio	Quadratic	0.6023	2	0.3011	5249.61	< 0.0001	0.9994	Suggested
	Cubic	0.0003	2	0.0001	7.07	0.0349	0.9999	Aliased

According to the sum of squares of the models (**Table 3**), the quadratic equation was found to be the best match for the encapsulation efficiency and swelling ratio because the p-values for these models were less than 0.05, and were not aliased. The resulting encapsulation efficiency equation in terms of the coded factor is as follows:

$$Y_1 = 8.75 + 9.50X_1 + 0.29X_2 + 0.002025X_1X_2 - 0.49X_1^2 - 0.0007X_2^2 \quad (7)$$

and the equation for swelling ratio is as follows:

$$Y_2 = -0.68 + 0.26X_1 + 0.011X_2 + 0.00012X_1X_2 - 0.014X_1^2 - 0.00003X_2^2 \quad (8)$$

where Y' is the encapsulation efficiency, and Y" is the swelling ratio. X_1 and X_2 represent time and power variables, respectively. A positive sign indicates a synergistic effect and a negative sign indicates an antagonistic effect [33]. Thus, it can be seen that X_1, X_2, and X_1X_2 have a significant influence on the encapsulation efficiency and swelling ratio, whereas X_1^2 and X_2^2 have small impacts. The results will increase to a certain level as time and power increase. However, because the quadratic effect and interactions between independent variables have a negative effect, under certain variable conditions, the encapsulation efficiency and swelling ratio value will tend to decrease.

Table 4 Analysis of variance (ANOVA) for response surface quadratic model.

Dependent Variable	Source	Sum of Squares	dF	Mean Square	F Value	*p*-value Prob > F	
%EE	Model	545.34	5	109.07	1167.92	< 0.0001	significant
	X_1-Time	76.28	1	76.28	816.84	< 0.0001	
	X_2-Power	12.48	1	12.48	133.64	< 0.0001	
	X_1X_2	1.48	1	1.48	15.81	0.0054	
	X_1^2	136.91	1	136.91	1466.03	< 0.0001	
	X_2^2	369.09	1	369.09	3952.31	< 0.0001	
	Residual	0.6537	7	0.0934			
	Lack of Fit	0.2899	3	0.0966	1.06	0.458	not significant
	Pure Error	0.3638	4	0.0909			
	Cor Total	545.99	12				
	Std. Dev	0.3056					
	R^2	0.9988					
	R^2adjusted	0.9979					
	R^2predicted	0.9952					
Swelling ratio	Model	0.7217	5	0.1443	2516.38	< 0.0001	significant
	X_1-Time	0.0997	1	0.0997	1738.67	< 0.0001	
	X_2-Power	0.0148	1	0.0148	258.61	< 0.0001	
	X_1X_2	0.0049	1	0.0049	85.42	< 0.0001	
	X_1^2	0.1024	1	0.1024	1785.5	< 0.0001	
	X_2^2	0.5516	1	0.5516	9616.03	< 0.0001	
	Residual	0.0004	7	0.0001			
	Lack of Fit	0.0003	3	0.0001	4.09	0.1037	not significant
	Pure Error	0.0001	4	0			
	Cor Total	0.7221	12				
	Std. Dev	0.0076					
	R^2	0.9994					
	R^2adjusted	0.9990					
	R^2predicted	0.9968					

The relevance and fitness of the quadratic model were also determined using analysis of variance (ANOVA) and significance was judged by the *p*-value calculated from the data. When the *p*-value was smaller than 0.05, the main factors significantly affected the response. The *p*-value (probability of error value) is a tool for determining the significance of each regression coefficient and its interaction impact, as well as the interaction effect of each variable. The greater the significance of the associated coefficient, the lower the *p*-value [34]. Based on the ANOVA results in **Table 4**, the quadratic model proved significant. The quadratic effect of all independent variables significantly affected the encapsulation efficiency and swelling ratio ($p < 0.05$). The lack-of-fit F-values for efficiency (1.06) and swelling (4.09) indicated that the error was insignificant, with the probability of occurrence owing to noise being 45.80% and 10.37%, respectively. The high R-square values of 99.87% and 99.94%, respectively, indicate the

accuracy and robustness of the model in representing the data.

Based on the Pareto diagram (**Figures 2(a)** and **2(b)**), the linear and quadratic models of the independent variables were significant. The negative quadratic effect indicated that excessive increases in the independent variables actually decreased the encapsulation efficiency and swelling ratio. Conversely, the positive linear effects of the sonication time (X_1) and power (X_2) indicated that increasing these 2 variables could improve the encapsulation efficiency and swelling ratio. **Figure 2(c)** and d confirm that the developed model is highly accurate in predicting the encapsulation efficiency and swelling ratio. Data points located on or near the diagonal line (Y = X) indicate that the model fits the experimental data and the experimental residuals are normally distributed, ensuring that each point distribution is a good approximation [35].

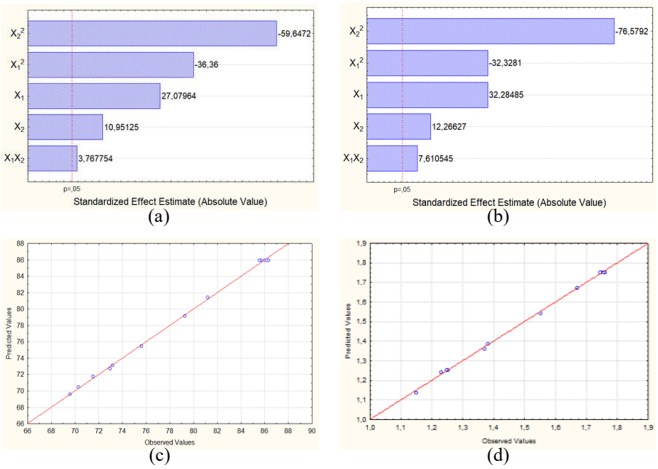

Figure 2 The influence of time (X_1) and power (X_2) on the (a) encapsulation efficiency and (b) swelling ratio is depicted in a pareto diagram; predicted (c) encapsulation efficiency; and (d) swelling ratio against observed (experimental).

Correlation of significant factor affecting encapsulation efficiency and swelling ratio

Figures 3 and **4** show that sonication time and power affect the encapsulation efficiency and swelling ratio of the curcumin beads and microcapsules. Increasing either variable generally improved both responses, but excessive sonication or ultrasonic intensity decreased them. The highest encapsulation efficiency (86.56%) and swelling ratio (1.781 g/g) were achieved after 10 min of sonication at 210 W, which was the optimal condition for curcumin beads.

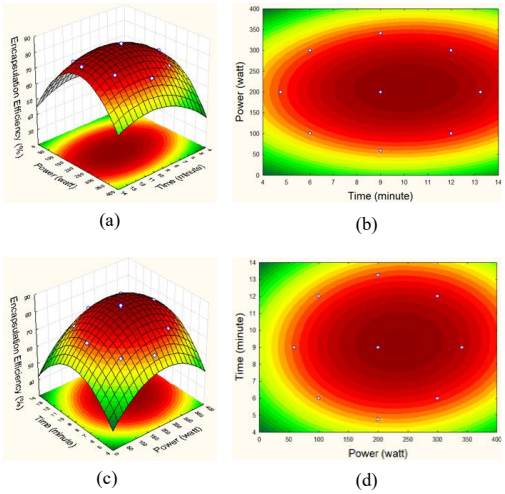

Figure 3 Time vs power (a) 3D surface; (b) contour plots and power vs time (c) 3D surface; (d) contour plots of the encapsulation efficiency.

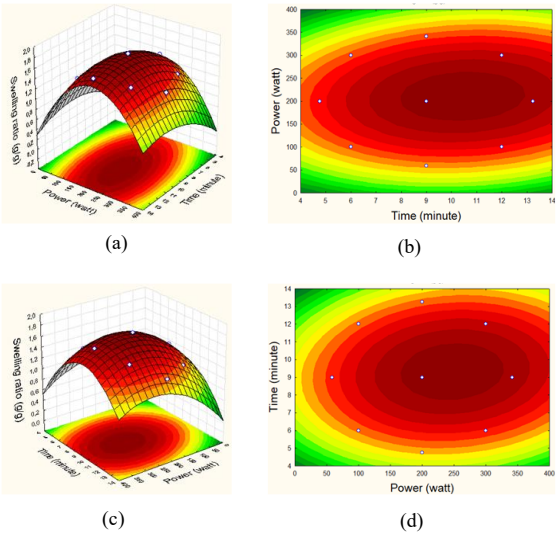

Figure 4 Time vs power (a) 3D surface; (b) contour plots and power vs time (c) 3D surface; (d) contour plots of the swelling ratio.

Model validation and optimization of encapsulation efficiency and swelling ratio

Validation was performed to ensure that the model and optimization results were obtained in triplicate. The experimental values were compared with the predicted values. The experimental results of the model validation and predictive values are listed in **Table 5**. The experimental encapsulation efficiency and swelling ratio using the model had only minor margins of error of 0.520% for encapsulation efficiency and 0.795% for swelling ratio. The optimization results and simulation revealed that the difference between the predicted value and the actual value was less than 5%, indicating that the correlation was good and that the optimization of the response surface methodology for predicting the encapsulation efficiency and swelling ratio was appropriate and feasible [35].

Table 5 Validation of experimental and predictive values under various operating conditions.

Dependent Variable	Factor		Response (%EE)			
	Time (min)	Power (W)	Observed	Predicted	Residual	Error (%)
%EE	10	210	87.185	86.560	0.625	0.717
	10	210	87.951	86.560	1.391	1.582
	10	210	85.925	86.560	−0.635	−0.739
					Average	0.520
Swelling ratio (g/g)	10	210	1.830	1.781	0.049	2.678
	10	210	1.783	1.781	0.002	0.135
	10	210	1.773	1.781	−0.008	−0.429
					Average	0.795

Particle size analysis

Particle size is typically the most critical characteristic used to reflect the physicochemical qualities of encapsulated materials for targeted nutrition and medicinal applications. **Figure 5** shows the particle size of the microcapsules.

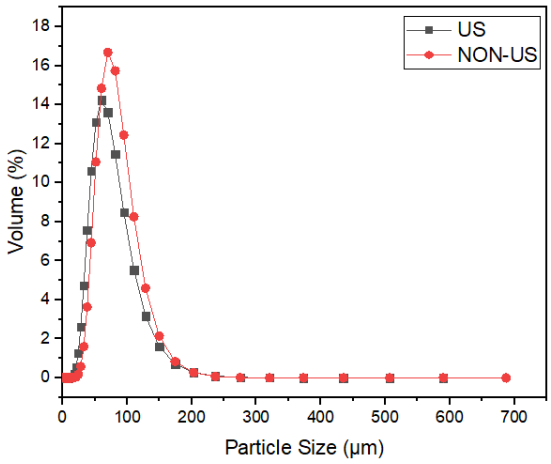

Figure 5 Particle size distribution of microcapsule under different conditions (ultrasound & non-ultrasound).

Ultrasound has been proven to be an effective technique for decreasing the particle size of homogenized complexes [36]. Their application notably decreases particle interactions, leading to substantial reductions in size [37]. According to Ding *et al.* [38], the rupture of non-covalent connections and disruption of protein aggregates as a result of the turbulence effect, cavitation, and strong shearing force caused by ultrasonic intensity are most likely responsible for the reduction in particle size after sonication treatment. In both the samples, the particle size distribution was unimodal, indicating a uniform distribution. However, the particle size distribution from the ultrasound treatment exhibited a narrower range than to that of the non-ultrasonicated sample. Ultrasound reduces repulsive forces and steric hindrances between molecules, thereby compacting the structure and decreasing particle size [39]. Additionally, the shear force resulting from bubble bursts owing to ultrasonic cavitation breaks down larger polymers, effectively reducing the molecular weight of the particles. This results in a narrower molecular weight distribution and, consequently, a decreased particle size [40].

Wang *et al.* [41] reported that the absence of ultrasonic treatment resulted in a sample with bimodal particle size distribution, indicating an irregular distribution of particle sizes. The introduction of ultrasonic treatment led to a reduction in the particle size, which was attributed to the shock waves generated by particle collisions within the emulsion and the collapse of cavitation bubbles. Qu *et al.* [42] supported this by asserting that ultrasonic treatment caused a decrease in microcapsule particle size. This is attributed to the potential of ultrasound to reduce the repulsive force and steric hindrance between molecules, resulting in a denser particle structure [43]. Additionally, Feng *et al.* [44] observed that appropriate ultrasonic treatment significantly reduced the particle size of nanodispersion.

FTIR analysis

The results of the FTIR analysis are shown in **Figure 6**. For comparison, FTIR analysis was performed on the best curcumin encapsulation and curcumin encapsulation without ultrasound treatment. In **Figure 6(a)**, the FTIR spectra of alginate and chitosan show the OH stretching at 3,367 cm^{-1}. The presence of the N-H bending vibration at the 1,617 cm^{-1} indicated the primary amino group of chitosan [45]. The peak at 1,426 cm^{-1} indicates symmetric vibration of the carboxylate group ($–COO^–$) [46]. Furthermore, low-intensity peaks were observed at 1,078 cm^{-1}, indicating the presence of phosphate groups (P=O) [47]. The FTIR spectrum of curcumin in **Figure 6(b)** displays infrared absorption peaks at wavelengths of 3,294 cm^{-1} (O-H), indicating the presence of free hydroxyl groups [48]. The absorption peak at 2,910 cm^{-1} signifies the C-H bonds in the aromatic rings [49]. Moreover, several other notable peaks are evident in the curcumin spectra, such as those at 1,631 cm^{-1} (C=C aromatic), 991 cm^{-1} (C-O-C stretching), and 758 cm^{-1} (C-H aromatic ring) [45].

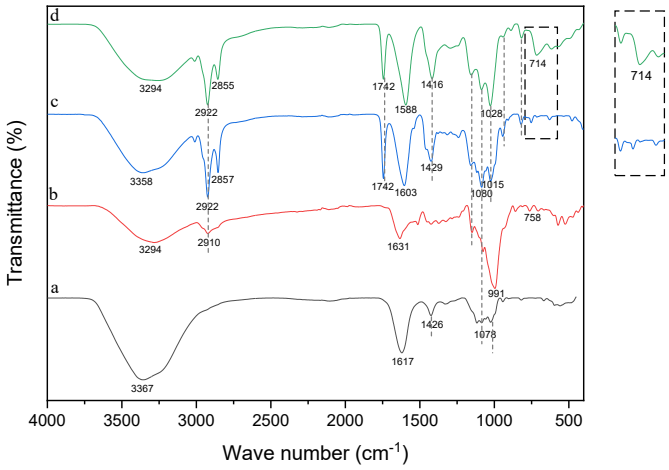

Figure 6 FTIR spectrum for (a) alginate/chitosan; (b) curcumin; (c) alginate/chitosan/curcumin (non-ultrasound); (d) alginate/chitosan/curcumin (ultrasound).

As can be seen in **Figures 6(c)** and **6(d)**, it was discovered that the vibrations of the C-H bond stretching [50], C-O-C stretching [45], and C-H bond stretching of the aromatic compounds in the curcumin [45] compounds in the curcumin [45] were responsible for the adsorption band widths between 2,922, 1,015, 1,028 and 714 cm^{-1}. This indicated that curcumin was encapsulated in the alginate-chitosan wall material. The characteristics of the functional groups of curcumin appeared to have been slightly affected by ultrasound treatment, as shown in **Figures 6(c)** and **6(d)**. As shown in the spectrum in **Figure 6(d)**, the alginate-chitosan-curcumin treated with ultrasound exhibited a greater peak intensity at 714 cm^{-1}, which revealed the C-H bond. In addition, the peak at 1,742 cm^{-1} representing the stretching vibration of the carbonyl group (C=O) of the soybean oil ester structure decreased in intensity after ultrasonication. Changes were also observed in the peak at 1,603 cm^{-1} which shifted to 1,588 cm^{-1} which corresponding to the vibration of the aromatic C=C and C=O groups of the diketo structure of curcumin. This shift reflects the increased homogenization and interaction between the lipid phase and curcumin due to increased hydrogen bonding and electrostatic interactions by sonication [39]. The more stable state of the hydrogen bonds reflects an increase in the interaction of the bioactive compound with the wall components. In other words, the ultrasonic treatment induces stronger hydrogen bonds between these components, which can improve [51]. According to Liu *et al.* [39], the physical forces of mechanical action from ultrasound can increase the rates of mass transfer, increasing the frequency of contact and collision between bioactive compounds and the wall material, thereby improving encapsulation efficiency. Liang *et al.* [52] noted that the encapsulation of bioactive substances within polysaccharides matrices strengthens intermolecular hydrogen bonds, leading to a significant increase in peak intensity.

SEM analysis

The surface morphology of the alginate/chitosan/curcumin beads was observed by SEM (**Figure 7**). SEM analysis allows the identification of cracks, pores, or changes in particle shape, the morphological structure of which greatly influences the stability and effectiveness of the product. SEM analysis was performed on the best curcumin encapsulation results and curcumin encapsulation without ultrasound treatment for comparison. In **Figure 7(a)**, it can be seen that the alginate/chitosan/curcumin beads had a rough surface without cracking. As shown in **Figure 7(b)**, the alginate/chitosan/curcumin beads had a crack on the surface. This can be attributed to the effects of ultrasound. Ultrasound is a versatile tool that can be finely adjusted across a wide frequency range, allowing precise control of the intensity and occurrence of cavitation events. This adaptability enables its application in regulating material characteristics, including the particle size, surface roughness, and internal structure [51].

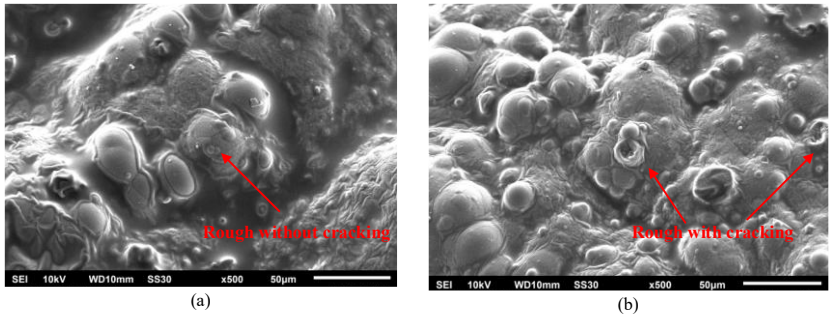

(a) (b)

Figure 7 Beads morphology of (a) alginate/chitosan/curcumin (non-ultrasound); (b) alginate/chitosan/curcumin (ultrasound).

SEM results revealed alterations on the surface of the sample beads subjected to ultrasound treatment. The changes observed on the bead surface can be attributed to cavitation, which generates elevated stresses and shear forces. This leads to the mechanical degradation of the amorphous layer in the wall material, ultimately reducing the particle size and resulting in numerous cracks on the bead surface. This phenomenon causes the disruption of glycosidic bonds and degradation of the carboxyl groups in alginate, causing the particle structure to relax and providing a larger space for the surrounding medium to penetrate the particles [53]. Furthermore, the cracks allow solvent entry more easily, accelerating the diffusion of curcumin out of the matrix, thus promoting the initial burst release. This effect can be advantageous for certain functional applications such as active substance delivery systems that require rapid release in the initial phase [54]. Similar instances of cracks were documented by Inui et al., where ultrasound-treated samples experienced damage due to ultrasound cavitation [55]. Ultrasonic treatment causes rupture and mechanical damage of beads through the collapse of cavitation bubbles, inducing high-pressure gradients and high local velocities of liquid layers in their vicinity, resulting in shear forces capable of damaging beads. This phenomenon was noticeable in the FTIR absorption spectrum, characterized by an intensified peak at 714 cm^{-1}, which is consistent with the observations reported by Prasetyaningrum *et al.* [56]. However, cracking negatively affect the shelf life of microcapsules. Cracks in capsule walls open pathways for oxygen, water vapor, and light, which can accelerate curcumin degradation during storage. This reduces the effectiveness of encapsulation in protecting the active compounds from environmental conditions. Therefore, cracking must be controlled by optimizing the intensity and duration of ultrasonication.

Curcumin release study

The cumulative release of bioactive curcumin from alginate-chitosan beads was studied in simulated gastric (pH 1.2) and intestinal (pH 6.8) fluids for 24 h. The release of bioactive curcumin from alginate-chitosan beads at pH 1.2 and 6.8 for 24 h is shown in **Figure 8**. The release of bioactive curcumin was faster at pH 6.8 than at pH 1.2. Alginate is sensitive to pH. Alginate expands at alkaline pH and shrinks at acidic pH. When the drug is coated with alginate, it is protected from the impact of the acidic environment of the stomach and delivered directly to the intestines [57]. At acidic pH, the alginate-chitosan beads showed low release because alginate was protonated and produced an insoluble form of alginic acid. Chitosan blocks this release, and the positively charged groups interact strongly with alginate, thereby preventing the release of bioactive curcumin. When the pH was increased to 6.8, the release of bioactive curcumin was higher than that at pH 1.2. This is associated with the speed of degradation of alginate-chitosan beads, where the speed of degradation of alginate-chitosan beads increases with increasing pH value.

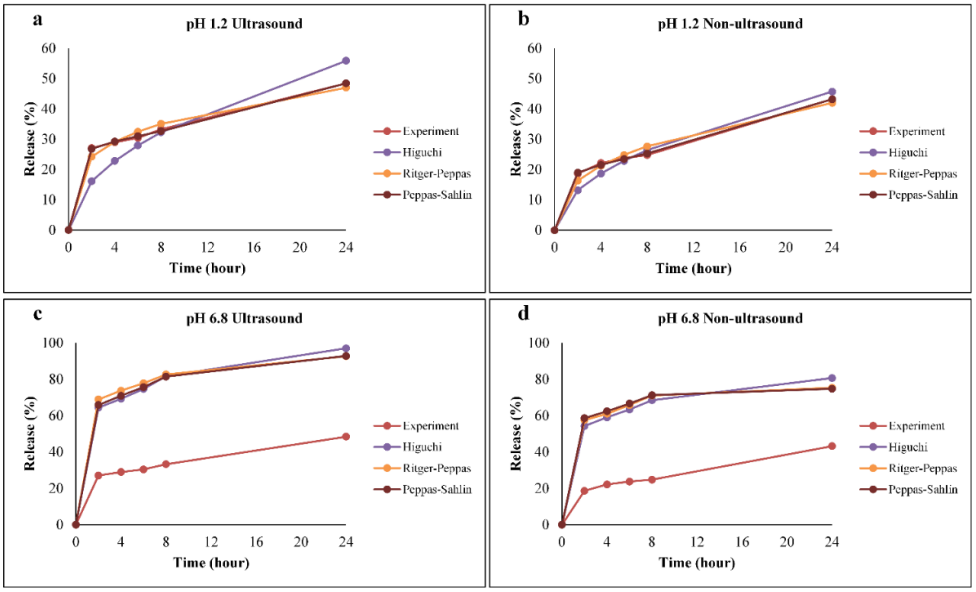

Figure 8 Release study of curcumin at pH 1.2 and 6.8.

Table 6 Release kinetics of curcumin bioactive compounds.

	Higuchi		Ritger-Peppas			Peppas-Sahlin				
	k_h	R^2	k_1	n	R^2	k_1	k_2	m	R/F	R^2
pH 1.2										
Ultrasound	11.41	0.953	20.13	0.271	0.993	24.74	0.23	0.15	0.0088	0.999
Non-ultrasonicated	9.35	0.984	12.59	0.383	0.991	16.85	0.19	0.19	0.0112	0.999
pH 6.8										
Ultrasound	22.37	0.889	49.93	0.176	0.999	50.32	0.02	0.18	0.0004	0.999
Non-ultrasonicated	21.76	0.894	47.32	0.177	0.999	50.47	0.08	0.14	0.0023	0.999

Table 6 shows that ultrasound-encapsulated beads had an enhanced release rate compared to non-ultrasound beads. This enhancement was attributed to the disruption of polymer bonds by sonication, thereby reducing the protective capacity of curcumin. Similar observations have been reported by Wardhani *et al.* [58]. The kinetic parameters of curcumin release from the alginate-chitosan hydrogel beads were analyzed using the Ritger-Peppas, Peppas-Sahlin, and Higuchi models. The Ritger-Peppas and Peppas-Sahlin models showed better statistical fit with high correlation coefficients than the Higuchi model, which lacks fit because it only describes a diffusion mechanism. An n value of approximately 0.17 in the Ritger-Peppas model indicates Fickian diffusion as the primary mechanism. Furthermore, the k_1 values for sonicated beads (pH 1.2 = 20.13; pH 6.8 = 49.93) were higher than those for non-ultrasonicated beads (pH 1.2 = 12.59; pH 6.8 = 47.31), indicating that sonication increases the rate of curcumin release. The Peppas-Sahlin model showed that Fickian diffusion dominates the release process, with k_1 values greater than k_2 and a low relaxation factor. The R/F ratio values were lower in ultrasound beads (pH 1.2 = 0.0088; pH 6.8 = 0.0004) than in non-ultrasonicated beads (pH 1.2 = 0.0112; pH 6.8 = 0.0023), indicating an increased contribution from diffusion. Degradation of alginate-chitosan facilitates the release of curcumin due to polymer chain cleavage, as evidenced by the decrease in R/F values with sonication. The use of ultrasonic waves increases the solubility of alginate-chitosan by cleaving the polymer chains. Consequently, the degraded polymer exhibited a reduced encapsulation efficacy, thereby accelerating the release of bioactive compounds.

For oral applications, the release system must be adapted to the transit time and pH of the human gastrointestinal tract. In the stomach, the pH is highly acidic (approximately 1.2), and curcumin is unstable

under these conditions. Therefore, early release must be suppressed to prevent the degradation of the active ingredient. Ideally, the encapsulation system releases only < 30% of curcumin in the first 0 - 120 min at pH 1.2 as an initial burst release, while the remaining curcumin remains protected. After reaching the small intestine (pH 6.8), which lasts approximately 120 - 240 min, curcumin release should occur gradually and continuously to increase its bioavailability. At this pH, the system exhibited higher n and k_1 values, supporting a controlled primary release (> 80%). Ultrasonication allows the capsule to survive in an acidic environment and only releases its contents significantly when it reaches a neutral pH, thus aligning with the goal of targeted delivery.

Conclusions

This study demonstrated that varying ultrasonic time and power significantly influenced the encapsulation efficiency and physicochemical properties of alginate/chitosan-based curcumin microcapsules. The optimum condition was achieved at 10 min of sonication with a power of 210 W, resulting in an encapsulation efficiency of up to 86.56% and a swelling ratio of 1.781. FTIR analysis confirmed a shift in the C=C/C=O band from 1,603 to 1,588 cm^{-1} after ultrasonication, indicating stronger interactions within the alginate/chitosan matrix. SEM analysis showed morphological changes in the form of cracks on the rough surface of the beads due to ultrasonic cavitation. Particle size analysis showed that ultrasonication produced a narrower distribution in the 10 - 50 µm range compared to the non-ultrasonicated sample which had a wider distribution. The release of curcumin fits better with the Peppas-Sahlin model with a dominant diffusion mechanism, where the sonicated beads have a higher k_1 value so that the bioactive release rate is faster. Additionally, the lower R/F ratio of the Peppas-Sahlin model on the ultrasonic bead indicated a predominant release via diffusion.

Acknowledgements

The authors gratefully acknowledge the financial support of the Ministry of Education and Culture of the Republic of Indonesia through the Riset Publikasi International Bereputasi Tinggi (RPIBT) 2024 research scheme.

Declaration of Generative AI in Scientific Writing

The authors declare that they have not used Artificial Intelligence (AI) tools in the creation of this article.

CRediT author statement

Aji Prasetyaningrum: Supervision; Project administration, funding acquisition, Conceptualization; Methodology. **Aulia Dwi Ashianti**: Writing- Original draft; Investigation; Software; Formal analysis. **Nur Rokhati**: Conceptualization and Validation. **Moh Djaeni**: Conceptualization and Validation. **Dani Puji Utomo**: Writing-Review & Editing; Visualization; Data Curation; Resources.

References

[1] V De Leo, AM Maurelli, L Giotta, V Daniello, S Di Gioia, M Conese, C Ingrosso, F Ciriaco and L Catucci. Polymer encapsulated liposomes for oral co-delivery of curcumin and hydroxytyrosol. *International Journal of Molecular Sciences* 2023; **24(1)**, 790.

[2] D Carrozza, G Malavasi, E Ferrari and MC Menziani. Alginate beads containing cerium-doped mesoporous glass and curcumin: Delivery and stabilization of therapeutics. *International Journal of Molecular Sciences* 2023; **24**, 880.

[3] M Saifullah, MRI Shishir, R Ferdowsi, MRT Rahman and Q Van Vuong. Micro and nano encapsulation, retention and controlled release of flavor and aroma compounds: A critical review. *Trends in Food Science and Technology* 2019; **86**, 230-251.

[4] SS Patel, HA Pushpadass, MEE Franklin, SN Battula and P Vellingiri. Microencapsulation of curcumin by spray drying: Characterization and fortification of milk. *Journal of Food Science and Technology* 2021; **59(4)**, 1326-1340.

[5] MV Traffano-Schiffo, M Castro-Giraldez, PJ Fito, M Perullini and PR Santagapita. Gums induced microstructure stability in Ca(II)-alginate beads containing lactase analyzed by SAXS. *Carbohydrate Polymers* 2018; **179**, 402-407.

[6] DU Kapoor, A Pareek, S Sharma, BG Prajapati, K Thanawuth and P Sriamornsak. Alginate gels: Chemistry, gelation mechanisms, and therapeutic applications with a focus on GERD treatment.

International Journal of Pharmaceutics 2025; **675**, 125570.

[7] M Szekalska, K Sosnowska, A Czajkowska-Kośnik and K Winnicka. Calcium chloride modified alginate microparticles formulated by the spray drying process: A strategy to prolong the release of freely soluble drugs. *Materials* 2024; **11(9)**, 1522.

[8] S Afzal, M Maswal and AA Dar. Rheological behavior of pH responsive composite hydrogels of chitosan and alginate: Characterization and its use in encapsulation of citral. *Colloids and Surfaces B: Biointerfaces* 2018; **169**, 99-106.

[9] D Thomas, M Latha and KK Thomas. Alginate/chitosan nanoparticles for improved oral delivery of rifampicin: Optimization, characterization and *in vitro* evaluation. *Asian Journal of Chemistry* 2018; **30(4)**, 736-740.

[10] Y Chen, Y Lu, RJ Lee and G Xiang. Nano encapsulated curcumin: And its potential for biomedical applications. *International Journal of Nanomedicine* 2020; **15**, 3099-3120.

[11] N Choudhury, M Meghwal and K Das. Microencapsulation: An overview on concepts, methods, properties and applications in foods. *Food Frontiers* 2021; **2**, 426-442.

[12] E Gürbüz, B Keresteci, C Günneç and G Baysal. Encapsulation applications and production techniques in the food industry techniques in the food industry. *Journal of Nutrition and Health Sciences* 2020; **7(1)**, 106.

[13] L Pudziuvelyte, M Marksa, K Sosnowska, K Winnicka, R Morkuniene and J Bernatoniene. Freeze-drying technique for microencapsulation of *Elsholtzia ciliata* ethanolic extract using different coating materials. *Molecules* 2020; **25**, 2237.

[14] I Buljeta, A Pichler, J Šimunović and M Kopjar. Polysaccharides as carriers of polyphenols: Comparison of freeze-drying and spray-drying as encapsulation techniques. *Molecules* 2022; **27**, 5069.

[15] R Rajam and P Subramanian. Encapsulation of probiotics: Past, present and future. *Beni-Suef University Journal of Basic and Applied Sciences* 2022; **11(1)**, 46.

[16] P Sacco, S Pedroso-Santana, Y Kumar, N Joly, P Martin and P Bocchetta. Ionotropic gelation of chitosan flat structures and potential applications. *Molecules* 2021; **26(3)**, 660.

[17] F Matter, AL Luna and M Niederberger. From colloidal dispersions to aerogels: How to master nanoparticle gelation. *Nano Today* 2020; **30**, 100827.

[18] N Omer, YM Choo, N Ahmad and NSM Yusof. Ultrasound-assisted encapsulation of pandan (*Pandanus amaryllifolius*) extract. *Ultrasonics Sonochemistry* 2021; **79**, 105793.

[19] L Perrin, S Desobry-Banon, G Gillet and S Desobry. Review of high-frequency ultrasounds emulsification methods and oil/water interfacial organization in absence of any kind of stabilizer. *Foods* 2022; **11**, 2194.

[20] N Mehta, JS, P Kumar, AK Verma, P Umaraw, SK Khatkar, AB Khatkar, D Pathak, U Kaka and AQ Sazili. Ultrasound-assisted extraction and the encapsulation of bioactive components for food applications. *Foods* 2022; **11(19)**, 192973.

[21] J Su and A Cavaco-Paulo. Effect of ultrasound on protein functionality. *Ultrasonics Sonochemistry* 2021; **76**, 105653.

[22] F Zhao, X Liu, X Ding, H Dong and W Wang. Effects of high-intensity ultrasound pretreatment on structure, properties, and enzymolysis of soy protein isolate. *Molecules* 2019; **24**, 3637.

[23] X Wang, X Ni, C Duan, R Li, X Jiang, M Xu and R Yu. The effect of ultrasound treatment on the structural and functional properties of tenebrio molitor myofibrillar protein. *Foods* 2024; **13**, 172817.

[24] J Qiu, H Zhang and Z Wang. Ultrasonic degradation of polysaccharides from *Auricularia auricula* and the antioxidant activity of their degradation products. *LWT - Food Science and Technology* 2019; **113**, 108266.

[25] P Kour, S Afzal, A Gani, MI Zargar, UN Tak, S Rashid and AA Dar. Effect of nanoemulsion-loaded hybrid biopolymeric hydrogel beads on the release kinetics, antioxidant potential and antibacterial activity of encapsulated curcumin. *Food Chemistry* 2022; **376**, 131925.

[26] X Ren, T Hou, Q Liang, X Zhang, D Hu, B Xu, X Chen, M Chalamaiah and H Ma. Effects of

frequency ultrasound on the properties of zein-chitosan complex coacervation for resveratrol encapsulation. *Food Chemistry* 2019; **279**, 223-230.

[27] H Liu, J Zhang, H Wang, Q Chen and B Kong. High-intensity ultrasound improves the physical stability of myofibrillar protein emulsion at low ionic strength by destroying and suppressing myosin molecular assembly. *Ultrasonics Sonochemistry* 2021; **74**, 105554.

[28] WF Huang, GCP Tsui, CY Tang and M Yang. Optimization strategy for encapsulation efficiency and size of drug loaded silica xerogel/polymer core-shell composite nanoparticles prepared by gelation-emulsion method. *Polymer Engineering and Science* 2018; **58**, 742-751.

[29] Y Liu, S Wang, W Lan and W Qin. Development of ultrasound treated polyvinyl alcohol/tea polyphenol composite films and their physicochemical properties. *Ultrasonics Sonochemistry* 2019; **51**, 386-394.

[30] Y Wang, C Ai, H Wang, C Chen, H Teng, J Xiao and L Chen. Emulsion and its application in the food field: An update review. *eFood* 2023; **4**, 102.

[31] AG Alvarado, M Arellano, M Rabelero, JE Puig and JC Sánchez-Díaz. Effect of particle size on the swelling and compression modulus of nanostructured polyacrylamide hydrogels. *Journal of Macromolecular Science, Part A: Pure and Applied Chemistry* 2015; **52(5)**, 381-386.

[32] R Ebrahimi. The study of factors affecting the swelling of ultrasound-prepared hydrogel. *Polymer Bulletin* 2019; **76**, 1023-1039.

[33] A Prasetyaningrum, W Widayat, B Jos, R Ratnawati, T Riyanto, GR Prinanda, BU Le Monde and EE Susanto. Optimization of sequential microwave-ultrasonic-assisted extraction of flavonoid compounds from *Moringa oleifera*. *Trends in Sciences* 2023; **20(1)**, 6401.

[34] EW Gibson. The role of *p*-values in judging the strength of evidence and realistic replication expectations. *Statistics in Biopharmaceutical Research* 2021; **13(1)**, 6-18.

[35] N Zhao and M Wang. Research on parameter optimization of the express warehousing and distribution system based on the box-behnken response surface methodology. *Advances in Civil Engineering* 2021; **2021(1)**, 8723017.

[36] Y Li, G Xu, W Li, L Lv and Q Zhang. The role of ultrasound in the preparation of zein nanoparticles/flaxseed gum complexes for the stabilization of pickering emulsion. *Foods* 2021; **10(9)**, 1990.

[37] O Gul, FT Saricaoglu, I Atalar, LB Gul, F Tornuk and S Simsek. Structural characterization, technofunctional and rheological properties of sesame proteins treated by high-intensity ultrasound. *Foods* 2023; **12(9)**, 1791.

[38] Q Ding, G Tian, X Wang, W Deng, K Mao and Y Sang. Effect of ultrasonic treatment on the structure and functional properties of mantle proteins from scallops (*Patinopecten yessoensis*). *Ultrasonics Sonochemistry* 2021; **79**, 105770.

[39] Y Liu, Q Liang, X Liu, H Raza, H Ma and X Ren. Treatment with ultrasound improves the encapsulation efficiency of resveratrol in zein-gum arabic complex coacervates. *LWT - Food Science and Technology* 2022; **153**, 112331.

[40] X Zhu, RS Das, ML Bhavya, M Garcia-Vaquero and BK Tiwari. Acoustic cavitation for agri-food applications: Mechanism of action, design of new systems, challenges and strategies for scale-up. *Ultrasonics Sonochemistry* 2024; **105**, 106850.

[41] X Zhu, RS Das, ML Bhavya, M Garcia-Vaquero and BK Tiwari. Effect of high-intensity ultrasound on the physicochemical properties, microstructure, and stability of soy protein isolate-pectin emulsion. *Ultrasonics Sonochemistry* 2021; **82**, 105871.

[42] W Qu, Y Feng, T Xiong, A Qayum and H Ma. Preparation, structural and functional characterization of corn peptide-chelated calcium microcapsules using synchronous dual frequency ultrasound. *Ultrasonics Sonochemistry* 2023; **102**, 106732.

[43] W Qu, T Guo, X Zhang, Y Jin, B Wang, H Wahia and H Ma. Preparation of tuna skin collagen-chitosan composite film improved by sweep frequency pulsed ultrasound technology. *Ultrasonics Sonochemistry* 2021; **82**, 105880.

[44] S Feng, X Zheng, D Luan, P Shao and P Sun. Preparation and characterization of zein-based phytosterol nanodispersions fabricated by

ultrasonic assistant anti-solvent precipitation. *LWT - Food Science and Technology* 2019; **107**, 138-144.

[45] ABD Nandiyanto, R Oktiani and R Ragadhita. How to read and interpret FTIR spectroscope of organic material. *Indonesian Journal of Science and Technology* 2019; **4(1)**, 97-118.

[46] N Pilipenko, OH Goncalves, E Bona, IP Fernandes, JA Pinto, GD Sorita, FV Leimann and MF Barreiro. Tailoring swelling of alginate-gelatin hydrogel microspheres by crosslinking with calcium chloride combined with transglutaminase. *Carbohydrate Polymers* 2019; **223**, 115035.

[47] Suryani, NHA Halid, NI Akib, Rahmanpiu and N Mutmainnah. Preparation of curcumin nanoparticle by using reinforcement ionic gelation technique. *AIP Conference Proceedings* 2017; **1838**, 020013.

[48] E Afzali, T Eslaminejad, SE Yazdi Rouholamini, M Shahrokhi-Farjah and M Ansari. Cytotoxicity effects of curcumin loaded on chitosan alginate nanospheres on the KMBC-10 spheroids cell line. *International Journal of Nanomedicine* 2021; **16**, 579-589.

[49] X Wang, X He and X Wang. FTIR analysis of the functional group composition of coal tar residue extracts and extractive residues. *Applied Sciences* 2023; **13(8)**, 5162.

[50] ABD Nandiyanto, AS Wiryani, A Rusli, A Purnamasari, AG Abdullah, I Widiaty and R Hurriyati. Extraction of curcumin pigment from Indonesian local turmeric with its infrared spectra and thermal decomposition properties. *IOP Conference Series: Materials Science and Engineering* 2017; **180**, 012136.

[51] L Meena, NAN Gowda, CK Sunil, A Rawson and S Janghu. Effect of ultrasonication on food bioactive compounds and their bio-accessibility: A review. *Journal of Food Composition and Analysis* 2024; **126**, 105899.

[52] Q Liang, X Sun, H Raza, MA Khan, H Ma and X Ren. Fabrication and characterization of quercetin loaded casein phosphopeptides-chitosan composite nanoparticles by ultrasound treatment: Factor optimization, formation mechanism, physicochemical stability and antioxidant activity. *Ultrasonics Sonochemistry* 2021; **80**, 105830.

[53] SR Falsafi, Y Maghsoudlou, M Aalami, SM Jafari and M Raeisi. Physicochemical and morphological properties of resistant starch type 4 prepared under ultrasound and conventional conditions and their *in-vitro* and *in-vivo* digestibilities. *Ultrasonics Sonochemistry* 2019; **53**, 110-119.

[54] D Yonata, YNS Ulvie, E Soesanto, E Sulistyowati, B Pranata and A Rosidi. Stabilization and controlled release of curcumin from temulawak by spray-drying microencapsulation with composite wall materials. *Trends in Sciences* 2025; **22(2)**, 9125.

[55] A Inui, A Honda, S Yamanaka, T Ikeno and K Yamamoto. Effect of ultrasonic frequency and surfactant addition on microcapsule destruction. *Ultrasonics Sonochemistry* 2020; **70**, 105308.

[56] A Prasetyaningrum, BS Wicaksono, A Hakiim, AD Ashianti, SFC Manalu, N Rokhati, DP Utomo and M Djaeni. Ultrasound-assisted encapsulation of citronella oil in alginate/carrageenan beads: characterization and kinetic models. *ChemEngineering* 2023; **7(1)**, 10.

[57] H Thai, C Thuy Nguyen, L Thi Thach, M Thi Tran, HD Mai, TTT Nguyen, GD Le, M Van Can, LD Tran, GL Bach, K Ramadass, CI Sathish and QV Le. Characterization of chitosan/alginate/ lovastatin nanoparticles and investigation of their toxic effects *in vitro* and *in vivo*. *Scientific Reports* 2020; **10(1)**, 909.

[58] DH Wardhani, FN Etnanta, HN Ulya and N Aryanti. Iron encapsulation by deacetylated glucomannan as an excipient using the gelation method: Characteristics and controlled release. *Food Technology and Biotechnology* 2022; **60(1)**, 41-51.